

First-order chiral to non-chiral transition in the angular dependence of the upper critical induction of the Scharnberg-Klemm p -wave pair state

Jingchuan Zhang^{1,2,*}, Christopher Lörcher², Qiang Gu¹, and Richard A. Klemm^{2†}
¹*Department of Physics, University of Science and Technology Beijing, Beijing 100083, China*
²*Department of Physics, University of Central Florida, Orlando, FL 32816-2385 USA*

(Dated: February 28, 2024)

We calculate the temperature T and angular (θ, ϕ) dependence of the upper critical induction $B_{c2}(\theta, \phi, T)$ for parallel-spin superconductors with an axially symmetric p -wave pairing interaction pinned to the lattice and a dominant ellipsoidal Fermi surface (FS). For all FS anisotropies, the chiral Scharnberg-Klemm state $B_{c2}(\theta, \phi, T)$ exceeds that of the chiral Anderson-Brinkman-Morel state, and exhibits a kink at $\theta = \theta^*(T, \phi)$, indicative of a first-order transition from its chiral, nodal-direction behavior to its non-chiral, antinodal-direction behavior. Applicability to Sr_2RuO_4 , UCoGe , and topological superconductors such as $\text{Cu}_x\text{Bi}_2\text{Se}_3$ is discussed.

I. INTRODUCTION

Recently, there has been a great deal of interest in p -wave superconductivity^{1–9,11–25}. The most likely candidate p -wave superconductors are the ferromagnetic superconductors UGe_2 , UCoGe , and URhGe , which exhibit long-range ferromagnetism well above the superconducting transition temperature T_c , and the same electrons participate in the ferromagnetism and the superconductivity^{1–7}. In URhGe , measurements of the temperature T dependence of the upper critical induction $B_{c2}(T)$ in the three crystal axis directions was found to fit the Scharnberg-Klemm theory of the p -wave polar state with completely broken symmetry (CBS)^{3,8}, with single-component p_z -pairing state only along the crystal a -axis. Subsequent experiments found a reentrant superconducting phase at much higher magnetic field \mathbf{H} strengths, violating the conventional Pauli limit $B_P = 1.85T_c$ (T/K) by a factor of 20. B_{c2} in UCoGe also violates B_P by a factor of 20, but its anisotropy suggests that if the superconductivity were p -wave, it would be more likely to have an axial state form, such as do the chiral Anderson-Brinkman-Morel (ABM) and chiral Scharnberg-Klemm (SK) states^{26–29}. Second, there has been an even greater interest in Sr_2RuO_4 , as the Knight shift measurements for \mathbf{H} parallel and perpendicular to the layers all showed no temperature T dependence below T_c , suggestive of a parallel-spin state^{11,12}. However, B_{c2} experiments on that material were shown to be strongly Pauli limited for $\mathbf{B} \perp \hat{c}$ ^{13–17,19,30}, and scanning tunneling microscopy experiments showed strong evidence for a nodeless gap¹⁸, although with cylindrical Fermi surfaces (FSs), this might be consistent with an axial p -wave state. Third, there has been a large recent interest in topological insulators, in the hope that they might become chiral p -wave superconductors with doping, applied pressure, or proximity coupling^{20–25}. Initial $B_{c2}(T)$ measurements on $\text{Cu}_x\text{Bi}_2\text{Se}_3$ were consistent with a p -wave polar state for \mathbf{H} both parallel and perpendicular to the layers^{23,26}. However, scanning tunneling microscopy (STM) experiments established that $\text{Cu}_x\text{Bi}_2\text{Se}_3$ has an isotropic gap strongly suggestive of an s -wave order parameter (OP)²⁵,

and that isotropic s -wave OP was respectively proximity-induced up to 7 K and 50 K into Bi_2Se_3 layers deposited atop the c -axes of the layered low- T_c and high- T_c superconductors, 2H-NbSe_2 and $\text{Bi}_2\text{Sr}_2\text{CaCu}_2\text{O}_{8+\delta}$ ^{32,33}, consistent with s -wave substrate crystal OPs in the c -axis direction of both of those layered superconductors^{31,34–36}. However, still undiscovered topological superconductors might have axial p -wave OP symmetry.

Previously, we generalized the microscopic calculation of $B_{c2}(T)$ for the p -wave polar state pinned to a crystal lattice direction to extend its validity to a superconductor with a dominant ellipsoidal FS and \mathbf{B} in an arbitrary direction, $\mathbf{B} = B(\sin \theta \cos \phi, \sin \theta \sin \phi, \cos \theta)$, with respect to the crystal lattice, in order to provide a sound theoretical basis for a more sensitive probe of the actual OP in orthorhombic materials such as URhGe . Here we use the same technique to construct a theory of the full angular dependence of $B_{c2}(\theta, \phi, T)$ for the ABM and SK states, in order to identify the symmetry of the OP in UCoGe , Sr_2RuO_4 , and other candidate materials. Since UCoGe is orthorhombic, the ellipsoidal FS model is the best that can be made without additional features such as magnetic pairing fluctuation effects and \mathbf{B} dependencies of the pairing interactions³⁷, or \mathbf{B} -dependent interactions³⁸, *etc.* For tetragonal Sr_2RuO_4 , the lack of any detectable ferromagnetism strongly suggests weak coupling interactions, but there are three barrel shaped FSs, and the STM experiments strongly suggest nearly equal isotropic gaps on each¹⁸. Although one could envision a scenario in which one FS dominated $B_{c2}(0^\circ, \phi, T)$ and another dominated $B_{c2}(90^\circ, \phi, T)$, since the latter is of primary interest, it suffices to consider only one FS. Moreover, as the k_z dispersion of those bands is sufficient to avoid dimensional crossover effects in $B_{c2}(90^\circ, \phi, T)$ measurements^{15,31,39,40}, an ellipsoid of uniaxial anisotropy is sufficient to examine B_{c2} measurements for all \mathbf{B} directions with high accuracy³¹. As anticipated earlier, for a parallel-spin pairing interaction of the form $V(\mathbf{k}, \mathbf{k}') = 3V_0(\hat{k}_1\hat{k}'_1 + \hat{k}_2\hat{k}'_2)$, one would expect $B_{c2}(\theta, \phi, T)$ to be given by the SK state^{9,26}. Although a favorite pair state for Sr_2RuO_4 has the form $\hat{z}(\hat{k}_1 + i\hat{k}_2)$, where the \mathbf{d} -vector \hat{z} corresponds to the antiparallel-spin

state in the lattice representation, we shall here assume that the spins are parallel²⁶, and will include Pauli limiting effects subsequently³⁰. Here we present detailed calculations of the $B_{c2}(\theta, \phi, T)$ for both the ABM and SK states on a single ellipsoidal FS.

We assume weak coupling for a clean homogeneous type-II parallel-spin p -wave superconductor with effective Hamiltonian^{9,26},

$$\mathcal{H} = \sum_{\mathbf{k}, \sigma=\pm} a_{\mathbf{k}, \sigma}^\dagger [\epsilon(\mathbf{k} - e\mathbf{A}) - \mu] a_{\mathbf{k}, \sigma} + \frac{1}{2} \sum_{\mathbf{k}, \mathbf{k}', \sigma} a_{\mathbf{k}', \sigma}^\dagger a_{\mathbf{k}, \sigma}^\dagger V(\hat{\mathbf{k}}, \hat{\mathbf{k}}') a_{\mathbf{k}, \sigma} a_{\mathbf{k}', \sigma}, \quad (1)$$

$$V(\hat{\mathbf{k}}, \hat{\mathbf{k}}') = \frac{3}{2} V_0 \sum_{\sigma'=\pm} f_{\sigma'}(\hat{\mathbf{k}}) \hat{\mathbf{d}}_{\sigma'} \cdot \hat{\mathbf{d}}_{\sigma'}^* f_{\sigma'}^*(\hat{\mathbf{k}}'), \quad (2)$$

where we assume parallel-spin pairing with $\hat{\mathbf{d}}_{\sigma'} = \hat{\mathbf{x}} + i\sigma'\hat{\mathbf{y}}$ and $f_{\sigma'}(\hat{\mathbf{k}}) = (\hat{k}_1 + i\sigma'\hat{k}_2)$ from the degenerate Γ_3^- and Γ_4^- tetragonal point group representations¹⁰, e is the electronic charge, μ is the chemical potential, the unit wave vectors \hat{k}_i were previously defined on an ellipsoidal FS⁹, and we set $\hbar = k_B = 1$. For non-ferromagnetic candidate p -wave superconductors, the upper critical induction $B_{c2} = \mu_0 H_{c2}$, where H_{c2} is the upper critical field. After performing the Klemm-Clem (KC) transformations⁴¹ that map the ellipsoidal FS onto a spherical one and then rotate the transformed induction to the new \tilde{z} axis direction, the transformed linear gap equation becomes

$$\bar{\Delta}(\tilde{\mathbf{R}}, \hat{\mathbf{k}}) = T \sum_{\omega_n} \frac{N(0)}{2} \int d\Omega_{\tilde{\mathbf{k}}} \tilde{V}(\hat{\mathbf{k}}, \hat{\mathbf{k}}') \int_0^\infty d\xi_{\tilde{\mathbf{k}}} \times e^{-2\xi_{\tilde{\mathbf{k}}}'|\omega_n|} e^{-i\xi_{\tilde{\mathbf{k}}}' v_F \hat{\mathbf{k}}' \cdot \tilde{\mathbf{R}}} \bar{\Delta}(\tilde{\mathbf{R}}, \hat{\mathbf{k}}'), \quad (3)$$

where $\bar{\Delta}$ is the transformed Δ amplitude without the gauge phases⁹, $N(0) = mk_F/(2\pi^2)$ is the density of states per spin at the chemical potential μ for an effectively isotropic metal with a geometric mean mass $m = (m_1 m_2 m_3)^{1/3}$, effective Fermi wave vector $k_F = \sqrt{2m\mu}$, effective Fermi velocity $v_F = k_F/m$, and $\tilde{\mathbf{R}} = -i\alpha \tilde{\mathbf{R}} - 2e\tilde{\mathbf{A}}(\tilde{\mathbf{R}})$, where $\alpha(\theta, \phi) = \sqrt{\bar{m}_3} \sqrt{\cos^2 \theta + \gamma^{-2}(\phi) \sin^2 \theta}$, $\bar{m}_i = m_i/m$, and $\gamma^2(\phi) = \frac{m_3}{m_1 \cos^2 \phi + m_2 \sin^2 \phi}$ is the ellipsoidal anisotropy function⁹. The KC transformations change $V(\hat{\mathbf{k}}, \hat{\mathbf{k}}')$ in Eq. (2) to

$$\tilde{V}(\hat{\mathbf{k}}, \hat{\mathbf{k}}') = \frac{3}{2} V_0 \sum_{\sigma=\pm} \tilde{f}_\sigma(\hat{\mathbf{k}}) \tilde{f}_\sigma^*(\hat{\mathbf{k}}') \quad (4)$$

where $\tilde{f}_\sigma(\hat{\mathbf{k}}) = \hat{k}_1 + i\sigma(\hat{k}_2 \cos \theta' + \hat{k}_3 \sin \theta')$, $\cos \theta' = \sqrt{\bar{m}_3} \cos \theta / \alpha$, etc.⁹ From the form of $\tilde{V}(\hat{\mathbf{k}}, \hat{\mathbf{k}}')$, $\bar{\Delta}(\tilde{\mathbf{R}}, \hat{\mathbf{k}}) = \sum_{\sigma=\pm} \bar{\Delta}_\sigma(\tilde{\mathbf{R}}) \tilde{f}_\sigma(\hat{\mathbf{k}})$, we expand the $\bar{\Delta}_\sigma(\tilde{\mathbf{R}})$ in terms of the harmonic oscillator eigenfunctions $|n(\tilde{\mathbf{R}})\rangle$, $\bar{\Delta}_\sigma(\tilde{\mathbf{R}}) = \sum_{n=0}^\infty a_n^\sigma |n(\tilde{\mathbf{R}})\rangle$, perform the integrals over the \hat{k}_i vari-

ables in the linearized gap equation, and obtain this double recursion relation for the $a_n^{(\pm)}$,

$$\begin{aligned} a_n^{(\pm)} &= \left(\frac{1}{2} (1 + \cos^2 \theta') a_n^{(\pm)} + \frac{1}{2} \sin^2 \theta' a_n^{(\mp)} \right) \alpha_n^{(a)} \\ &+ \frac{1}{2} \sin^2 \theta' (a_n^{(\pm)} - a_n^{(\mp)}) \alpha_n^{(p)} \\ &+ \left(\frac{1}{4} \sin^2 \theta' a_{n+2}^{(\pm)} + \frac{1}{4} (1 \pm \cos \theta')^2 a_{n+2}^{(\mp)} \right) \beta_n \\ &+ \left(\frac{1}{4} \sin^2 \theta' a_{n-2}^{(\pm)} + \frac{1}{4} (1 \mp \cos \theta')^2 a_{n-2}^{(\mp)} \right) \beta_{n-2} \end{aligned} \quad (5)$$

where

$$\begin{aligned} \alpha_n^{(p,a)} &= \pi T \sum_{\omega_n} \int_0^\pi d\theta_{\tilde{\mathbf{k}}} \sin \theta_{\tilde{\mathbf{k}}} \left(3 \cos^2 \theta_{\tilde{\mathbf{k}}}', \frac{3}{2} \sin^2 \theta_{\tilde{\mathbf{k}}}' \right) \\ &\times \int_0^\infty d\xi_{\tilde{\mathbf{k}}} e^{-2\xi_{\tilde{\mathbf{k}}}'|\omega_n|} e^{-\eta_{\tilde{\mathbf{k}}}'/2} L_n(\eta_{\tilde{\mathbf{k}}'}), \quad (6) \\ \beta_n &= \pi T \sum_{\omega_n} \int_0^\pi d\theta_{\tilde{\mathbf{k}}} \frac{3}{2} \sin^3 \theta_{\tilde{\mathbf{k}}} \int_0^\infty d\xi_{\tilde{\mathbf{k}}} e^{-2\xi_{\tilde{\mathbf{k}}}'|\omega_n|} \\ &\times e^{-\eta_{\tilde{\mathbf{k}}}'/2} (-\eta_{\tilde{\mathbf{k}}}') L_n^{(2)}(\eta_{\tilde{\mathbf{k}}}') [(n+1)(n+2)]^{-1/2} \end{aligned} \quad (7)$$

where

$$\eta_{\tilde{\mathbf{k}}}' = eB\alpha(\theta, \phi) v_F^2 \xi_{\tilde{\mathbf{k}}}^2 \sin^2 \theta_{\tilde{\mathbf{k}}}', \quad (8)$$

$t = T/T_c$, $T_c = (2e^C \omega_0 / \pi) \exp(-1/N(0)V_0)$, ω_0 is a characteristic pairing cutoff frequency, $C \approx 0.5772$ is Euler's constant, and $L_n(z)$ and $L_n^{(2)}(z)$ are a Laguerre and an associated Laguerre polynomial, respectively^{9,26}.

For the chiral ABM state, the decoupled $a_n^{(\pm)}$ each satisfy $a_n^{(\pm)} D_n = \Gamma_n a_{n+2}^{(\pm)} + \Gamma_{n-2} a_{n-2}^{(\pm)}$, where $D_n = 1 - \frac{1}{2}(1 + \cos^2 \theta') \alpha_n^{(a)} - \frac{1}{2} \sin^2 \theta' \alpha_n^{(p)}$ and $\Gamma_n = \frac{1}{4} \sin^2 \theta' \beta_n$. Solving this recursion relation, we obtain the continued fraction expression from which $B_{c2}(\theta, \phi, t)$ for the ABM state is obtained numerically,

$$D_0 - \frac{\Gamma_0^2}{D_2 - \frac{\Gamma_2^2}{D_4 - \dots}} = 0. \quad (9)$$

As for the polar/CBS state⁹, one iteration is accurate to a few percent, but four or five iterations are needed for the accuracy necessary to observe the interesting effects.

The results for the reduced $b_{c2}(\theta, t)$ for a parallel-spin superconductor in the p -wave ABM state with a dominant spherical $\gamma^2(\phi) = 1$ FS are shown in Fig. 1. In Fig. 1(a), the curves for $\theta = 0^\circ(\mathbf{b} \parallel \hat{\mathbf{c}})$ (nodal direction) to $90^\circ(\mathbf{b} \perp \hat{\mathbf{c}})$ (antinodeal direction) are shown in increments of 10° . The result for the nodal direction ($\theta = 0^\circ$) was obtained previously²⁶. Just below T_c , $b_{c2}(\theta, \phi, t) \propto [m_3 \cos^2 \theta + 2\gamma^{-2}(\phi) \sin^2 \theta]^{-1/2}$, where the factor 2 arises from the ABM order parameter (OP) anisotropy. In order to distinguish which part of the overall $b_{c2}(\theta, t)$ anisotropy that is attributable solely to the order parameter anisotropy, in Fig. 1(b), those Fig. 1(a) results scaled to have the same slope at $t = 1$ are presented. Nothing unusual is evident from these spherical

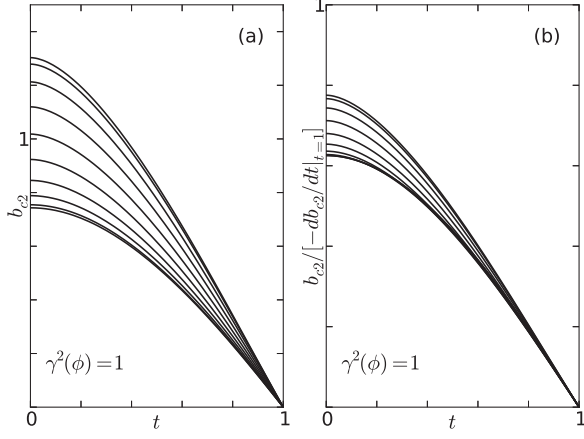


FIG. 1: (a) Reduced b_{c2} versus $t = T/T_c$ for the chiral ABM state [Eq. (9)] at θ values from 0° ($\mathbf{H} \parallel \hat{\mathbf{c}}$, bottom) to 90° ($\mathbf{H} \perp \hat{\mathbf{c}}$, top), in increments of 10° for a spherical FS. (b) Same curves normalized to have the same slopes at T_c .

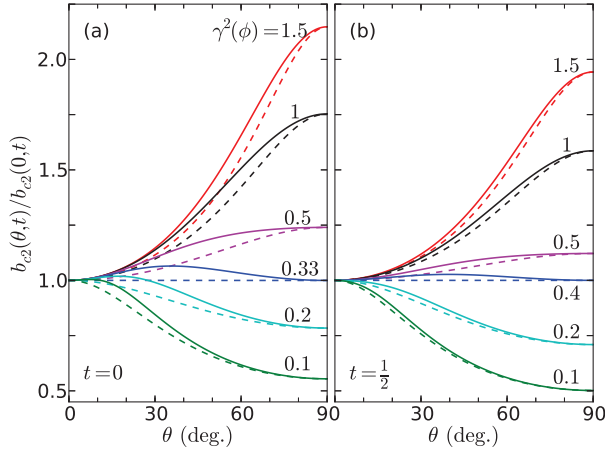


FIG. 2: (color online) Reduced b_{c2} versus θ for the chiral ABM state [Eq. (9)] at the indicated effective mass anisotropy $\gamma^2(\phi)$ values (solid) and the effective mass angular fits [Eq. (10), dashed] at $t = 0$ (a) and $t = 1/2$ (b).

FS curves, and they are smooth and increase monotonically with increasing θ .

However, we also studied the role of ellipsoidal (or uniaxial) FS anisotropy. In Fig. 2, we chose fixed FS anisotropy values $\gamma^2(\phi)$ ranging from 0.1 to 1.5 and plotted in Figs. 1 (a,b) at $t = 0$ and $1/2$, respectively. The solid curves are evaluated from Eq. (9). The dashed curves are the conventional “effective mass” anisotropy $b_{\text{eff}}(\theta, t)$ forms obtained by fitting the calculated $b_{c2}(0^\circ, t)$ and $b_{c2}(90^\circ, t)$,

$$b_{\text{eff}}(\theta, t) = [\cos^2 \theta / b_{c2}^2(0^\circ, t) + \sin^2 \theta / b_{c2}^2(90^\circ, t)]^{-1/2} \quad (10)$$

We note that $b_{c2}(\theta, t)$ exhibits an unusual θ dependence, with a peak in at θ^* for $\gamma^2(\phi) < 1/2$ that is distinctly different than the conventional b_{c2} maxima at $\theta = 0^\circ$ or 90° .

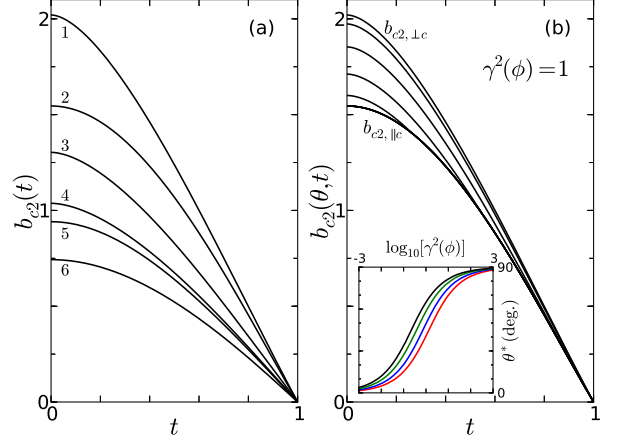


FIG. 3: (color online) (a) $b_{c2}(t)$ for the antinodal SK state (1), nodal SK state (2), antinodal ABM state (3), s-wave state absent of Pauli limiting (4), planar nodal (CBS) state (5), and nodal ABM state (6) on a spherical FS. (b) Reduced $b_{c2}(t)$ for the chiral SK state at θ values from 0° ($\mathbf{B} \parallel \hat{\mathbf{c}}$, bottom) to 90° ($\mathbf{B} \perp \hat{\mathbf{c}}$, top), in increments of 10° for a spherical FS. The $\theta = 0^\circ, 10^\circ, 20^\circ, 30^\circ$ and 40° are indistinguishable on this scale. Inset: Plots of the kink angle θ^* versus $\log_{10}[\gamma^2(\phi)]$ from top to bottom for $t = 3/4$ (black), $1/2$ (green), $1/4$ (blue), 0 (red).

Such anomalous double peaks at unconventional θ values satisfying $0 < \theta^* < 90^\circ$, and by reflection symmetry about 90° , also for $90^\circ < \theta^* < 180^\circ$, were predicted earlier for the polar state pinned to the lattice⁹. However, in that case, the anomalous double peaks were predicted to occur for $\lambda(t) > \gamma^2(\phi) > 3$, with maximal $\lambda(t)$ values for finite t . Since the anomalous behavior is unlikely to be relevant to either Sr_2RuO_4 or UCoGe , for which $\gamma^2 \gg 1$, for brevity, the $\lambda'(t)$ curve defining the lower limit of the range of θ^* for $\lambda'(t) < \gamma^2(\phi) < 1/2$ will be presented elsewhere³⁰.

The much more interesting chiral axial p -wave state is the SK state. We note that it is chiral as long as $\Delta^{(+)} \neq \Delta^{(-)}$, or $a_n^{(+)} \neq a_n^{(-)}$ for at least one relevant n value⁹. It is easy to see that for $\theta' = 0$, Eq. 5) reduces for $a_n^{(+)} \neq 0$ to $[1 - \alpha_n^{(a)}][1 - \alpha_{n+2}^{(a)}] = \beta_n^2$, which for $a_n^{(+)} \neq 0$ is the expression for the SK state with \mathbf{B} in the nodal direction²⁶, whereas for $\theta' = \pi/2$, it reduces for $a_n^{(+)} \neq a_n^{(-)}$ to $\alpha_n^{(p)} = 1$, the expression for the SK state with \mathbf{B} in the antinodal (polar state) direction²⁶.

However, for a general θ' , $a_n^{(+)} \neq a_n^{(-)}$, Eq. (5) is a double recursion relation in the six harmonic oscillator amplitudes, $a_n^{(\pm)}$, $a_{n+1}^{(\pm)}$ and $a_{n-2}^{(\pm)}$, which requires further analysis to write the exact solution. We first write $\Psi_n^{(\pm)} = \frac{1}{2}(a_n^{(+)} \pm a_n^{(-)})$, $D_n^{(+)} = 1 - \alpha_n^{(a)}$, $D_n^{(-)} = 1 - \alpha_n^{(a)} \cos^2 \theta' - \alpha_n^{(p)} \sin^2 \theta'$, and construct $\phi_n^{(\pm)} = \cos \theta' D_n^{(+)} \Psi_n^{(+)} \pm D_n^{(-)} \Psi_n^{(-)}$. After letting $n \rightarrow n + 2$ in the expression for $\phi_n^{(-)}$, we obtain two equations for $\Psi_n^{(+)}$ and $\Psi_{n+2}^{(+)}$ in terms of $\Psi_n^{(-)}$ and $\Psi_{n+2}^{(-)}$. Using these equa-

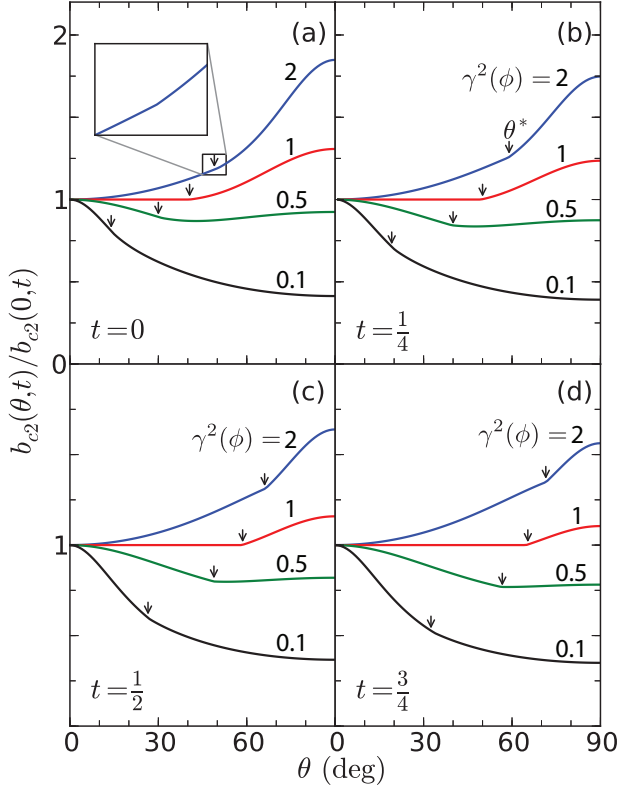


FIG. 4: (color online) Reduced upper critical induction b_{c2} versus θ for the chiral SK state for $\gamma^2(\phi) = 2$ (blue, top), 1 (red), 0.5 (green), and 0.1 (black) at $t = 0$ (a), $\frac{1}{4}$ (b), $\frac{1}{2}$ (c), and $\frac{3}{4}$ (d). The arrows indicate kinks in $b_{c2}(\theta)$ at θ^* , signifying first-order transitions from the chiral SK state ($\theta < \theta^*$) to the non-chiral antinodal SK (or polar) state $b_{c2}(t)$ curve ($\theta > \theta^*$).

tions to eliminate $\Psi_n^{(+)}$ and $\Psi_{n+2}^{(+)}$ in favor of $\Psi_n^{(-)}$ and $\Psi_{n+2}^{(-)}$, letting $n \rightarrow n - 2$ in the expression for $\Psi_{n+2}^{(-)}$, and equating that with the other expression for $\Psi_n^{(-)}$, we obtain the simple recursion relation for the $\Psi_n^{(-)}$, $A_n \Psi_{n+2}^{(-)} + B_n \Psi_n^{(-)} + C_n \Psi_{n-2}^{(-)} = 0$, the solution of which may be expressed in the continued fraction equation,

$$B_0 - \frac{A_0 C_0}{B_2 - \frac{A_2 C_2}{B_4 - \dots}} = 0, \quad (11)$$

where $B_n = B_n^{(+)} - B_n^{(-)}$, $A_n = E_{n-2} \beta_n [\cos^2 \theta' D_{n+2}^{(+)} - D_{n+2}^{(-)}]$, $B_n^{(+)} = D_n^{(-)} [E_n D_{n-2}^{(+)} + E_{n-2} D_{n+2}^{(+)}]$, $B_n^{(-)} = \cos^2 \theta' [\beta_n^2 E_{n-2} + \beta_{n-2}^2 E_n]$, $C_n = \beta_{n-2} E_n [\beta_{n-2} \cos^2 \theta' D_{n-2}^{(+)} - D_{n-2}^{(-)}]$, and $E_n = D_n^{(+)} D_{n+2}^{(+)} - \beta_n^2$. As for the polar/CBS state and the ABM state, one iteration is accurate to a few percent, but four or five iterations are necessary to display the most important features of this work. We also eliminated $\Psi_n^{(-)}$ and $\Psi_{n+2}^{(-)}$ in favor of $\Psi_n^{(+)}$ and $\Psi_{n+2}^{(+)}$, but the $b_{c2}(\theta, \phi, t)$ values calculated from the resulting continued fraction equation were always lower than those calculated from Eq. (11).

In Fig. 3(a), we plotted the reduced $b_{c2}(t)$ for the nodal and antinodal directions of the ABM, SK, and polar/CBS states, along with that [curve (4)] of a conventional s -wave superconductor without any Pauli limiting effects, all for a spherical FS. The antinodal directions of the polar state and SK states both have $b_{c2}(t)$ curves described by curve (1), and the nodal direction of the SK state $b_{c2}(t)$ follows curve (2), as found previously²⁶. Curve (3) is the new $b_{c2}(t)$ curve for the antinodal direction of the ABM state. Curves (5) and (6) describe the planar nodal polar/CBS state direction and the nodal direction of the ABM state, as also found previously⁸. We note that the SK state $b_{c2}(\theta, \phi, t)$ is larger for all field directions than is the ABM state $b_{c2}(\theta, \phi, t)$, as the second chiral component of the OP allows for the state to be superconducting at larger applied field strengths. In Fig. 3(b), the t dependence of $b_{c2}(\theta, t)$ is illustrated for $\theta = 0^\circ$ ($\mathbf{b} \parallel \hat{\mathbf{c}}$) (bottom) to $\theta = 90^\circ$ ($\mathbf{b} \perp \hat{\mathbf{c}}$) (top), in increments of 10° . Surprisingly, the curves for $\theta = 0^\circ, 10^\circ, 20^\circ, 30^\circ$ and 40° are remarkably close to one another, and appear to cross at finite t values! This is an indication of a chiral to non-chiral transition for $\theta \geq 40^\circ$ at various t values, as the vortices just below b_{c2} appear to lock onto the nodal direction for $\theta \leq 40^\circ$, but for $\theta > 40^\circ$ unlock from that direction, and favor the non-chiral antinodal (or polar) state direction. Similar behavior was predicted recently for the vortex structure in the mixed state of a chiral ABM state model of Sr_2RuO_4 ¹⁹.

To investigate this surprising feature in more detail, in Fig. 4 we show the θ dependence of $b_{c2}(\theta, \phi, t)$ at the effective mass anisotropy values $\gamma^2(\phi) = 0.1, 0.5, 1$, and 2 , at $t = 0, \frac{1}{4}, \frac{1}{2}$, and $\frac{3}{4}$. In every case, there is a kink in $b_{c2}(\theta)$ at $\theta = \theta^*$ for fixed ϕ and t , which we interpret as evidence for a first-order phase transition from a chiral to non-chiral state. Although these kinks are easiest to see for small γ^2 values, and Sr_2RuO_4 has $\gamma^2 > 10^3$, our high-accuracy solutions of Eq. (11) allow us to determine $\theta^*[\gamma^2(\phi), t]$ with great precision. In the inset to Fig. 3(b), we plotted θ^* in degrees versus $\ln_{10}[\gamma^2(\phi)]$ from -3 to 3 at the reduced t values $0, \frac{1}{2}, \frac{1}{4}$, and $\frac{3}{4}$. Thus, if Sr_2RuO_4 were a chiral p -wave parallel-spin superconductor as often purported, then one ought to observe a first order chiral to non-chiral transition for $\theta \approx 90^\circ$, nearly parallel to the layers. It is therefore quite interesting to note that some evidence for this sort of behavior may have already been observed in very recent $H_{c2}(T)$ measurement on Sr_2RuO_4 ¹⁷. However, a cautionary note that is that $b_{c2}(90^\circ, \phi, t)$ appears to be strongly Pauli limited^{13–16}, and more details of such and other fits using this FS model will soon become available³⁰.

With regards to the ferromagnetic superconductor UCoGe , the ferromagnetism in the c -axis direction allows for an axial-type parallel-spin p -wave pairing interaction, most likely mediated by ferromagnetic exchange interactions, in the ab plane. However, at large applied fields along the b -axis direction, not only does $B_{c2,b}(0)$ exceed the Pauli limit by a factor of at least 20, but the very strange behavior of $B_{c2,b}(T)$, including prelim-

inary evidence for an S -shaped curve, strongly suggests something akin to a reentrant superconducting phase overlapping the low-field phase, which would be similar to the two phases of URhGe. Fitting such behavior will require significant modifications to the theory, such as by including ferromagnetic fluctuations³⁷, field-dependent interactions³⁸, different FS shapes,^{43,44} and two ferromagnetically-split FSs, which modifications are currently under study⁴⁵. Although an axial p -wave topological superconductor is presently elusive, this theory could be useful to identify a future candidate material.

In summary, we have studied the two most-common versions of an axially-symmetric p -wave pair state, the Anderson-Brinkman-Morel (ABM) and Scharnberg-Klemm (SK) states. For all induction \mathbf{B} directions and temperatures T , the reduced (dimensionless) the SK state $B_{c2}(\theta, \phi, t)$ exceeds that of the ABM state. Surprisingly, for $0 \leq \theta \leq \theta^*$, the only θ -dependence of $B_{c2}(\theta, \phi, t)$ arises from effective mass anisotropy, but then

$B_{c2}(\theta)$ exhibits a kink at $\theta^*[t, \gamma^2(\phi)]$. Hence, it appears that there are two basic states evident in $b_{c2}(\theta, \phi, t)$: the nodal, chiral SK state for $-\theta^* \leq \theta \leq \theta^*$, and the antinodal, non-chiral polar state for $\theta^* \geq \theta \geq -\theta^*$.

Acknowledgments

The authors thank J.-P. Brison, A. DeVisser, A. D. Huxley, Y. Matsuda, and K. Scharnberg for useful discussions. This work was supported in part by the Florida Education Fund, the McKnight Doctoral Fellowship, a Chateaubriand Fellowship from the Embassy of France, UCF startup funds, the Specialized Research Fund for the Doctoral Program of Higher Education of China (no. 20100006110021) and by Grant no. 11274039 from the National Natural Science Foundation of China.

-
- * nuscire@gmail.com
† richard.klemm@ucf.edu
- ¹ N. T. Huy *et al.*, Phys. Rev. Lett. **99**, 067006 (2007).
 - ² A. de Visser *et al.*, Phys. Rev. Lett. **102**, 167003 (2009).
 - ³ F. Hardy and A. D. Huxley, Phys. Rev. Lett. **94**, 247006 (2005).
 - ⁴ F. Lévy, I. Sheikin, and A. Huxley, Nature Phys. **3**, 460 (2007).
 - ⁵ E. A. Yelland *et al.*, Nature Phys. **7**, 890 (2011).
 - ⁶ D. Aoki *et al.*, J. Phys. Soc. Jpn. **80**, 013705 (2011).
 - ⁷ D. Aoki and J. Flouquet, J. Phys. Soc. Jpn. **81**, 011003 (2012).
 - ⁸ K. Scharnberg and R. A. Klemm, Phys. Rev. Lett. **54**, 2445 (1985).
 - ⁹ C. Lörcher *et al.*, Phys. Rev. B **88**, 024504 (2013).
 - ¹⁰ T. M. Rice and M. Sigrist, J. Phys.: Condens. Matter **7**, L643 (1995).
 - ¹¹ A. P. Mackenzie and Y. Maeno, Rev. Mod. Phys. **75**, 657 (2003).
 - ¹² Y. Maeno *et al.*, J. Phys. Soc. Jpn. **81**, 011009 (2012).
 - ¹³ K. Deguchi, Z. Q. Mao, and Y. Maeno, J. Phys. Soc. Jpn. **73**, 1313 (2004).
 - ¹⁴ K. Machida and M. Ichioka, Phys. Rev. B **77**, 184515 (2008).
 - ¹⁵ S. Kittaka *et al.*, Phys. Rev. B **80**, 174514 (2009).
 - ¹⁶ C.-H. Choi, J. Kor. Phys. Soc. **56**, 933 (2010).
 - ¹⁷ S. Yonezawa, T. Kajikawa, and Y. Maeno, Phys. Rev. Lett. **110**, 077003 (2013).
 - ¹⁸ H. Suderow *et al.*, New. J. Phys. **11**, 093004 (2009).
 - ¹⁹ M. Ishihara *et al.*, Phys. Rev. B **87**, 224509 (2013).
 - ²⁰ L. Fu and E. Berg, Phys. Rev. Lett. **105**, 097001 (2010).
 - ²¹ X. L. Qi and S. C. Zhang, Rev. Mod. Phys. **83**, 1057 (2011).
 - ²² M. Kriener *et al.*, Phys. Rev. Lett. **106**, 127004 (2011).
 - ²³ T. V. Bay *et al.*, Phys. Rev. Lett. **108**, 057001 (2012).
 - ²⁴ K. Kirschenbaum *et al.*, Phys. Rev. Lett. **111**, 087001 (2013).
 - ²⁵ N. Levy *et al.*, Phys. Rev. Lett. **110**, 117001 (2013).
 - ²⁶ K. Scharnberg and R. A. Klemm, Phys. Rev. B **22**, 5233 (1980).
 - ²⁷ P. W. Anderson and P. Morel, Phys. Rev. **123**, 1911 (1961).
 - ²⁸ P. W. Anderson and W. F. Brinkman, Phys. Rev. Lett. **30**, 1108 (1973).
 - ²⁹ V. P. Mineev and K. V. Samokhin, *Introduction to Unconventional Superconductivity* (Gordon and Breach, New York, NK, 1999).
 - ³⁰ J. Zhang *et al.*, to be published.
 - ³¹ R. A. Klemm, *Layered Superconductors Volume 1* (Oxford University Press, Oxford, UK and New York, NY 2012).
 - ³² M. Wang *et al.*, Science **336**, 52 (2012).
 - ³³ E. Wang *et al.*, Nat. Phys. **9**, 620 (2013).
 - ³⁴ K. A. Mueller, BAPS.2011.MAR.J3.2
 - ³⁵ Q. Li *et al.*, Phys. Rev. Lett. **83**, 4160 (1999).
 - ³⁶ R. A. Klemm, Phil. Mag. **85**, 801 (2005).
 - ³⁷ T. Hattori *et al.*, Phys. Rev. Lett. **108**, 066403 (2012).
 - ³⁸ K. Hattori and H. Tsunetsugu, Phys. Rev. B **87**, 064501 (2013).
 - ³⁹ R. A. Klemm, A. Luther, and M. R. Beasley, Phys. Rev. B **12**, 877 (1975).
 - ⁴⁰ R. A. Klemm and K. Scharnberg, Phys. Rev. B **24**, 6361 (1981).
 - ⁴¹ R. A. Klemm and J. R. Clem, Phys. Rev. B **21**, 1868 (1980).
 - ⁴² E. Helfand and N. R. Werthamer, Phys. Rev. **147**, 288 (1966).
 - ⁴³ D. W. Youngner and R. A. Klemm, Phys. Rev. B **21**, 3890 (1980).
 - ⁴⁴ C. T. Rieck and K. Scharnberg, Physica B **163**, 670 (1990).
 - ⁴⁵ C. Lörcher *et al.*, unpublished.